1 Results

1.1 Transition from Spiking to Bursting

1.1.1 EAG channel expression modulates spiking-bursting transition

As it was discussed in Section **??** one possible mechanism behind transition of the R5 activity between tonic firing and bursting may be due to diurnal variation in expression of the ether-à-go-go (EAG) channel. EAG is permeable to potassium. During night expression of these channels is low compared to the day. As potassium current is hyperpolarizing, increased expression of EAG channels during day might potentially decrease excitability of the cell and thus, number of spikes per burst.

EAG channels are voltage-gated ion channels. The family of EAG channels contains several subtypes. Some of them are inactivating (i.e. contain inactivation gate), while others are non-inactivating (i.e. lack inactivation gate) [1]. The kinetic properties of these channels in *Drosophila* are not extensively documented in the literature. I was able to find only a single paper providing kinetic properties of these channels in *Drosophila* [2]. Although the original model of the EAG channel described in the paper is blocked by Ca^{2+}, for simlicity, the present work assumes that the gating mechanism depends only on membrane potential. This simplification can be justified for several reasons. First, the EAG channel family is diverse, and other studies have reported that these channels are voltage-gated [1]. Second, even if calcium does inactivate these channels, the termination of a burst after a single spike should primarily be mediated by channel activation. Therefore, calcium-dependent inactivation is unlikely to play a significant role in the transition from bursting to spiking in R5 neurons.

In the literature bursting models generally lack EAG channels. Thus, the channel was added to the implemented models to test the above-mentioned hypothesis. The parameters for EAG channel were adapted from [2], with few modifications that will be discussed below. The current through the channel is given by:

$$I_{\text{EAG}} = g_{\text{EAG}} m^2 (V - V_K)$$

where g_{EAG} is the conductance, V_K is reversal potential of potassium, and m is activation variable

governed by Equation **??**. The units are omitted here, as they are model-specific and match those provided in Appendix **??**. The steady state activation $m_\infty(V)$, and activation time constant $\tau(V)$ are governed by:

$$m_\infty(V) = \left(\frac{1}{1 + \exp\left(-(V + 23.12 - d)/k\right)} \right) \tag{1.1}$$

$$\tau(V) = a \left(5497 - \frac{5500}{1 + \exp((V + 251.5 - d)/(-16.94 - 51.5))} \right) \tag{1.2}$$

Note, that Equation 1.1 lacks dependency on calcium, in contrast to the one proposed in [2]. In Equation 1.1 parameter k determines the slope of the sigmoid and was set to 16.94 in [2]. The parameters d and a were introduced in the current model to allow for a voltage shift in the functions, and to scale the time constant, respectively.

Several factors were considered when adjusting the parameters. First, if the region in steady state activation is nonzero within the interburst interval, it affects the oscillation period, as the potassium current opposes repolarization of the membrane potential, thus extending the period to reach the spiking threshold (see Figure ??? - add 1. Example of voltage traces, 2. magnitude of the total current within interburst interval). Second, the time constant should be fast enough to allow termination of the burst after the first spike. Note, that this is a strong condition, motivated by literature reporting tonic firing of R5 neurons during the daytime. However, further data analysis is needed, and it is possible that the assumption of tonic firing - and thus the above-mentioned requirement - may be revised (see Discussion).

Table **??** provides the exact parameter values used in the simulations. Figures **??** and **??** illustrate Equations 1.1 and 1.2, showing their dependence on membrane potential for parameter sets corresponding to different models (see also Figure **??** for the default parameters provided in [2]).

To investigate the transition between tonic spiking and bursting mediated by EAG channel, g_{EAG} was varied from 0 to 1 to reflect potential changes in channel expression between day and night(note, that maximal conductance reflects the number of ion channels in the conductance based model. See also Section **??**). To account for variations in external input during the day and night, the external current was also varied. All other parameters were set to their default values as specified in Section **??**. Figure 1 shows how the activity, interburst interval, and number of spikes per burst depend on g_{EAG} and external current for the model of thalamic relay

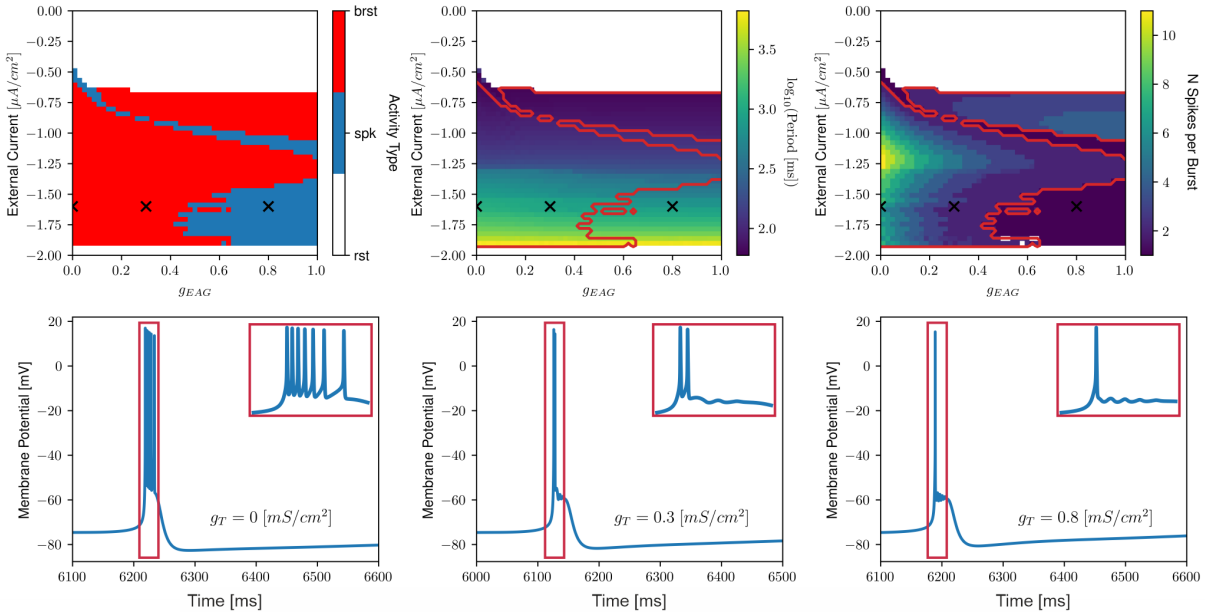

Figure 1: Spiking-to-Bursting Transition Induced by EAG Channels in Wang model. TEXT!!! + A-F. (A) Activity type; (B) Interburst period (here, tonic spiking is considered as one spike per burst), region where model showed two or more spikes per burst is outlied by red curve (corresponding to the red regions in (A); (C) number of spikes per burst); (D)-(F) examples of voltage traces in simulations. Corresponding parameter sets are denoted by "x" in (A)-(C). Insets shos the closeup of the spiking demonstrating that the number of spikes decreases with increasing g_{EAG}. For (D)-(F) the external input was set to -1.6 corresponding to the case when the model exhibits 1Hz bursting.

neuron proposed by Wang [16]. Activity is classified as bursting, spiking, or resting and was determined as described in Section **??**. For the purposes of analyzing interburst interval and spike count, tonic spiking was treated as a special case of bursting, consisting of one spike per burst.

For fixed ecternal input, the number of spikes mainly decrease with increasing g_{EAG} and the firing pattern switches from bursting to tonic firing for a critical value of g_{EAG}, while the period remains relatively constant (Figure 1A-C). Figures 1D-F further illustrate this effect by showing voltage traces from three representative simulations. The corresponding parameter combinations are indicated by 'x' in Figures 1A-C. Interestingly, there is a region in the phase space, where the number of spikes increase with increasing g_{EAG} (Figure 1C, upper boundary), however this region was not investigated within the scope of this thesis.

The results obtained from other models were qualitatively similar and are therefore not included in the main text (see Figures ??? in the Appendix).

1.1.2 Bifurcation analysis

In the previous section it was demonstrated that EAG channel may be responsible for termination of the burst and the emergence of tonic spiking–like behavior in R5 neurons. This section investigates the underlying mechanisms through bifurcation analysis.

Figure 2 presents the bifurcation analysis results for the model proposed by Wang [16], which generates bursting behavior mediated by T-type Ca^{2+} channels. In this model, the activation gate of the T-type channel is treated as instantaneous (see Section **??** for details), and the slow dynamics are governed by the inactivation gate, denoted by the variable h.To investigate how bursting depends on this variable, h was treated as a bifurcation parameter, while all other varialbes were allowed to evolve freely.

The analysis was performed for three representative values of g_{EAG} corresponding to the 'x' markers in Figure 1A-C. For each value of h, the stable and unstable fixed points were computed using AUTO-07P, along with the locations of Hopf and saddle-node (Saddle-Node (SN)) bifurcations. In Figure 2, stable and unstable fixed points are shown as solid and dashed black lines, respectively. Hopf bifurcations are indicated by circles, and saddle-node bifurcations by triangles. Periodic orbits were numerically continued from the Hopf bifurcations. The bursting trajectory was obtained by numerical simulations of the full system. Projection of the trajectory on V-h plane is overlaid as a green curve. The direction of the trajectory is indicated by black arrow at the bottom of the plots.

Figure 2A shows results in the absence of the EAG channels. The analysis is similar to the fast-slow decomposition discussed in Section **??**. The analysis follows a fast–slow decomposition similar to that described in Section **??**. However, before discussing the results, an important aspect should be highlighted.

Effect of another slow variable on fast-slow decomposition

From the perspective of fast-slow analysis, one might expect the full-system trajectory to closely follow the manifold of stable fixed points of the fast subsystem. However, the model contains an additional variable with a relatively slow timescale, associated to the Hyperpolarization-activated Cyclic Nucleotide-gated (HCN) channels (see Section ??? for the corresponding parameters). As discussed in Section **??**, HCN channels (referred to as "sag current" in [16]) are

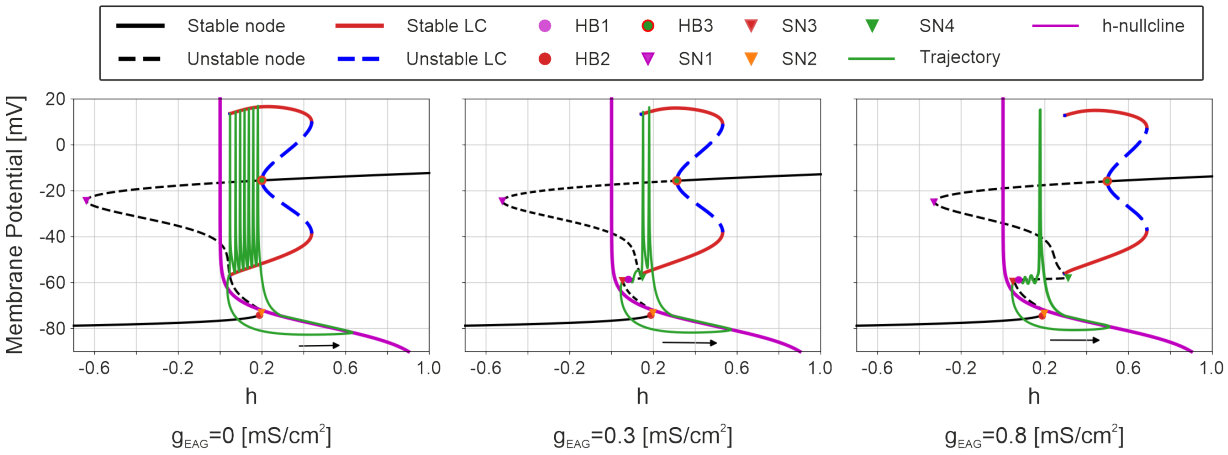

Figure 2: Transition from Spiking to Bursting via EAG channels. TEXT!!! + Make circles larger + A-C

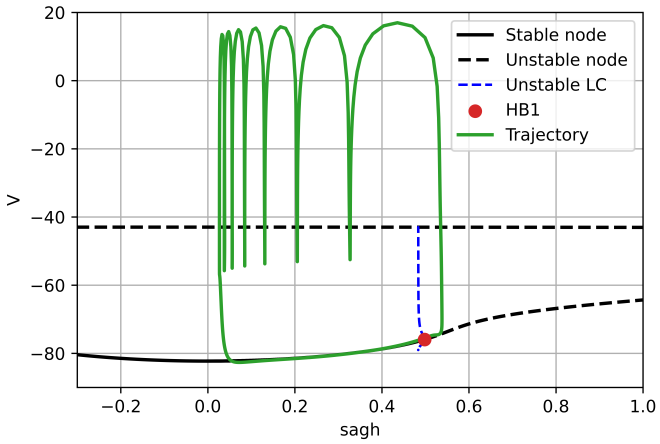

Figure 3: Bifurcation Diagram - Wang Model with Sag Activation as Bifurcation Parameter. TEXT!!!

hyperpolarization-activated channels that mediate depolarizing current, thus, they contribute to dynamics at relatively low values of membrane potential.

Notably, HCN channels contribute less during spiking phase. For example, at -55mV (approximately trough of the oscillation), the steady state activation has a value of ~ 0.12, decreasing to ~ 0.06 at -50mV and to ~ 0.016 at -40mV. Consequently, during spiking phase, the system behaves more like as the fast-slow in contrast to the resting state. This may explain why the bifurcation diagram seems to be more accurate in the spiking phase than in the resting phase of the reduced ("fast") subsystem without the h variable. Indeed, when the activation variable of the HCN channel was treated as a bifurcation parameter, the resulting trajectory closely fol-

lowed the manifold of stable fixed points in the reduced subsystem where the HCN activation was held constant (Figure 3).

To summarize, the transition of interest is from spiking to resting state, as EAG channels are considered to terminate bursts. Since the above analysis effectively captures the dynamics during the spiking phase, the approach remains suitable for investigating the mechanism.

Saddle-homoclinic orbit bifurcation underlies spiking-resting transition in Wang model

As shown in Figure 2A, the spiking phase is deminished when the stable limit cycle (indicated by solid red lines) collides with unstable node (dashed black lines). This is commonly referred to as saddle-homoclinic orbit bifurcation [11, 12] (see also Section **??**).

In the absence of EAG channels the trajectory is attracted by the stable limit cycle after the resting state of the reduced system (i.e. one without the h variable) looses stability, causing transition of the system to the spiking state. In spiking state, membrane potential provides a negative feedback to the variable h (note, that inactivation gate of T-type channels closes at depolarized potentials; see steady state inactivation function for the h gate in Figure **??**).

As g_{EAG} increases, the bifurcation point of the resting state remains unchanged (compare the onset of the bursts in Figure 2A-C). However, the point at which the limit cycle collides with the unstable nodes shifts to the right, and the system spends less time in the spiking regime. After g_{eag} reachis a critical value, the limit cycle disappears, and the system returns to the resting state via saddle-homoclinic orbit after a single spike.

Look at Bifurcation in Codim-2 ???

1.2 Oscillations after TTX Application

It was illustrated in Section **??** that R5 neurons exhibited slow oscillations, potentially mediated by Ca^{2+} channels after the sodium channels were blocked by application of Tetrodotoxin (TTX). These oscillations showed three main features: apparent afterhyperpolarization (AHP) (undershoot of the membrane potential below steady state), a spike with a width of approximately ~ 100ms, and a relatively long interspike interval on the order of seconds. Furthermore, no oscillations were present in Ca-$\alpha 1T$-KD animals after blockade of sodium channels.

As it was discussed in Section **??**, slow oscillations require either slow timescale, or the trajectory passing near the equilibrium of the full dynamical system. However, the latter scenario is generally not robust to parameter perturbations.

Out of the implemented models (see Section **??** and Appendix **??**), only two showed oscillations with apparent AHP - the one proposed by Wang [16] and Goldman [8] (for the latter parameters were taken from [6]). Plot examples of voltage traces. Neither model included gating mechanisms operating on timescales of seconds (see Appendix **??** for more details).

To investigate oscillations following sodium channel blockade in adapted neuronal models, several factors were considered. First, as it was discussed in Section **??**, knockdown of the T-type channels may have been partial rather than complete. Second, blockade of Na^{+} channels does not necessarily eliminate external input to the neuron. Apart from chemical synapses, neurons may receive external input via other mechanisms, such as gap-junctions, or passive leak channels. As such external effects can slightly vary across individuals, minor perturbations in parameteres, as well as external input, should not affect the dynamics. Therefore, in the adapted neuronal models all parameters were kept as specified in Section **??**, except for the maximal conductance of T-type channels (to account for the partial blockade) and the external input current. The spike period and with were calculated as described in Section **??**.

Figure 4 illustrates how the perid and the width of the spikes depend on the conductance of T-type channls and external input current. Note that for each model the label for the x axis was chosen to be the same as described in corresponding papers (g_T and g_{CaT}), although they all account for the T-type Ca^{2+} channel. The colored areas indcate parameter combinations where the neuron exhibited spiking activity, with the color scale representing either period (left column) or spike width (right column). White regions correspond to the parameter values where

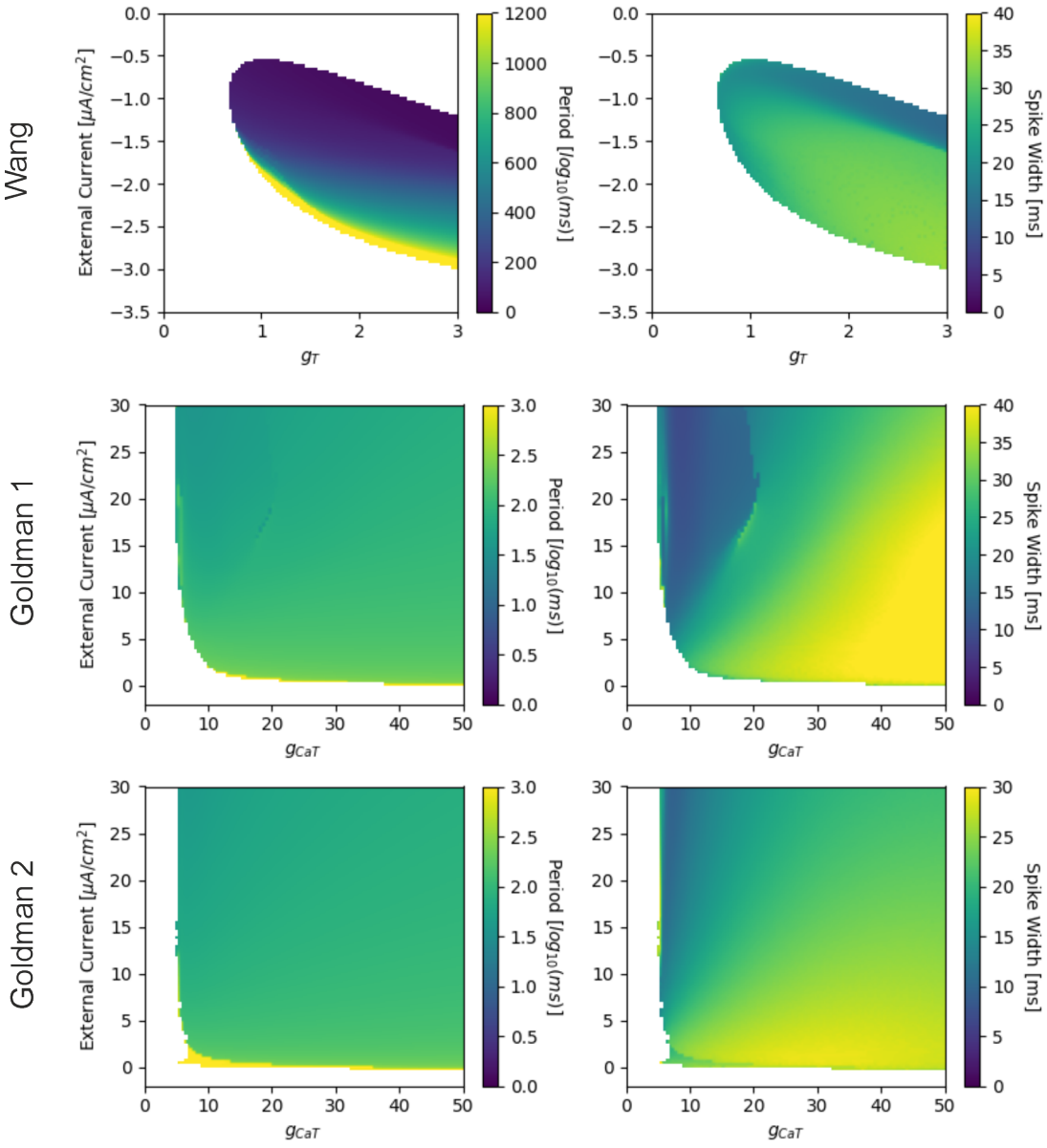

Figure 4: Effect of External Current and T-Type Conductance on Calcium Spike Width and Period. TEXT!!!. Colorbar label of the Wang is wrong, should be ms instead of log10(ms)!! Outline parts with ¿= 1sec period + units on x axis

the system did not exhibit spiking activity and converged to a resting state. In all three models the slow oscillations ($\geq$ 1 Hz) were confined to a narrow region of paramter space, close to bifurcation that separates spiking and resting regimes.

Thus, the results are consistent with the predictions outlined in Section **??**, and support the notion that the system requires an intrinsic slow variable to generate robust low-frequency oscillations. As discussed in Section **??**, a potential underlying slow mechanism may be the slow

removal of intracellular calcium following a spike, which could lead to the gradual inactivation of calcium-activated potassium channels. This, in turn, may contribute to the slow repolarization of the membrane potential between spikes.

On the other hand, it can be an ion channel which has time constant that is slow (of the order of seconds) at steady state and fast at depolarized states (of the order of several 10s of milliseconds).

1.3 Effects of T-Type Channel KD on Bursting

2 T-Type Calcium Channel

Main results:

- Estimated number of activation gates for Drosophila T-Type ion channels is 3.
- modeling the ion channel using Ohmic relationship between current and voltage did not procude good fits to observed current-voltage (I-V) relationship.
- The current-voltage relationship was reproduced when Goldman-Hodgkin-Katz (GHK) voltage flux equation was used instead of Ohmic current
- GHK equation models explicit relationship between current, voltage, temperature and intra-/extracellular ion concentrations.
- The fit of simulated I-V relatoinship to the observed data was improved when the steady-state activation function was shifted along V axis, and corresponding time constant was scaled and shifted along V axis (parameters for shifting and scaling were taken to be free parameters during optimization)

2.1 Model

T-Type Ca^{2+} current was modelled using constant-field equation [9]:

$$I_T(V) = m_T(V)^3 h_T(V) P z^2 \frac{VF^2}{RT} \frac{[Ca^{2+}]_{\text{inside}} - [Ca^{2+}]_{\text{outside}} \exp\left[-zFV/(RT)\right]}{1 - \exp\left[-zFV/(RT)\right]} \tag{2.1}$$

where m_T and h_T correspond to the activation and inactivation gates, P is the maximum permeability (scaled to either have the current amplitude observed during the electrophysiological experiments reported in [13] (Section 2.3), or to), z is the valence of ion ($= 2$ for Ca^{2+}), V is membrane potential in Volts, F is Faraday's constant ($\approx 9.6485 \times 10^4 C \cdot \text{mol}^{-1}$), R is the universal gas constant ($\approx 8.3145 J/K^\circ \cdot$Mol), T is temperature is Kelvin (here, $273.16+25 = 298.16^\circ$). $[Ca^{2+}]_{\text{inside}}$ and $[Ca^{2+}]_{\text{outside}}$ are the concentrations of Ca^{2+} inside and outside the membrane. The values were set to $23 \times e^{-9}$ and $0.5 \times e^{-3}$ correspondingly, from the motor neurons in Drosophila [7].

Another approach to model the T-Type Ca^{2+} current is by Ohm's law [9, 15]:

$$I_T(V) = g_T m_T(V)^3 h_T(V)(V - V_{Ca}) \tag{2.2}$$

g_T is the maximum value of the conductance of the T-Type Ca^{2+} current, and V_{Ca} us the reversal potential for Ca^{2+}, which can be estimated given the ion concentrations inside and outside the membrane (see Section 2.1.1). However, the model with the Ohmic current did not reprocude the I-V relations in [13] correctly (see Sction ...). Similar issue was described in [9], where choosing equation 2.1 instead of 2.2 resulted in better fit of the I-V relationship to the experimental data.

2.1.1 Reversal Potential

Reversal potential was estimated by Nernst equation [12]:

$$V_{\text{ion}} = \frac{RT}{zF} \ln \frac{[\text{Ion}]_{\text{outside}}}{[\text{Ion}]_{\text{inside}}}$$

where $[\text{Ion}]_{\text{inside}}$, and $[\text{Ion}]_{\text{outside}}$ are concentrations of the ions (here, Ca^{2+}) inside and outside of the cell. The values for $[Ca^{2+}]_{inside}$ and $[Ca^{2+}]_{outside}$ were taken to be $23nM$, and $0.5mM$ correspondingly from the motor neurons in Drosophila [14]. R is the universal gas constant ($\approx 8.3145 J/K^\circ \cdot$Mol), T is temperature is Kelvin (here, $273.16+25 = 298.16^\circ$), F is Faraday's constant ($\approx 9.6485 \times 10^4 C \cdot \text{mol}^{-1}$), z is the valence of the ion ($z = 2$ for Ca^{2+}).

$$V_{Ca} \approx 128mV$$

2.1.2 Activation Gate

Dynamics of the activation variable m_T of T-Type Ca^{2+} channel is given by [15]:

$$\frac{dm_T(V)}{dt} = \frac{m_{T,\infty}(V) - m_T(V)}{\tau_{m_T}(V)}$$

where [3, 15]:

$$m_{T,\infty}(V) = \frac{1}{1 + \exp\left[-(V - V_{m_T,1/2})/k_{m_T}\right]} \tag{2.3}$$

and

$$\tau_{m_T}(V) = \sigma_{m_T}(V)\tau^-_{m_T}(V) + (1 - \sigma_{m_T}(V))\tau^+_{m_T}(V) \tag{2.4}$$

In the equations above, $m_{T,\infty}$ and τ_{m_T} are voltage-sensitive steady-state activation function and time constant, correspondingly. $V_{m_T,1/2}$ is membrane potential at which the steady-state activation function is equal to its half-maximum (i.e. 0.5), and k_{m_T} is the slope factor. $\tau^-_{m_T}(V)$ and $\tau^+_{m_T}(V)$ describe the time constant below (deactivation) and above (activation) -50mV correspondingly, and $\sigma_{m_T}(V)$ defines smooth transition between the two at -50mV. First, the following functions were fit to the values provided in [13]:

$$\tau^-_{m_T}(V) = 3(a_{m_T,1} + \exp\left[(V - b_{m_T,1})/k_{m_T,1}\right]) \tag{2.5}$$

$$\tau^+_{m_T}(V) = a_{m_T,2} + \exp\left[-(V - b_{m_T,2})/k_{m_T,2}\right] \tag{2.6}$$

The scaling factor 3 for $\tau^-_{m_T}(V)$ is related to the how deactivation time constant was measured in [13] (for the details see Section 2.2.2). As the equations 2.5 have discontinuity at $V = -50$mV, after fitting the parameters of those equations, the following equation for $\sigma_{m_T}(V)$ was chosen to model smooth transition between the two:

$$\sigma_{m_T}(V) = \frac{1}{1 + \exp\left[c_{\tau_{m,T}}(v + 50)\right]} \tag{2.7}$$

where $c_{\tau_{m,T}} > 0$ controls the sharpness of the transition and was fitted to the combined activation and deactivation time constants from [13] after fixing the parameters of equation 2.5.

2.1.3 Inactivation Gate

Inactivation gate was modelled with first-order kinetic scheme [4, 5]:

$$\frac{dh_T(V)}{dt} = \frac{h_{T,\infty}(V) - h(V)}{\tau_{h_T}(V)}$$

where [4, 15]:

$$h_{T,\infty}(V) = \frac{1}{1 + \exp\left[(V - V_{h_T,1/2})/k_{h_T}\right]} \tag{2.8}$$

and [16]:

$$\tau_{h_T}(V) = h_{T,\infty}(V)(a_{h_T} + \exp\left[(V - b_{h_T})/k_{h_T}\right]) \tag{2.9}$$

Note 1. Second order kinetic schemes have also been developed for the inactivation gates [15].

The derivation of the equations in the paper are provided in more detail in Section **??**.

2.2 Fitting Data

As the data from the article is not available online, the values were estimated by taking screenshot, importing the image in Coreldraw and estimating the values using visual inspection and coordinate system of Coreldraw. The fitting was performed using python function *scipy.optimize.curve_fit*. The following plots show the estimated activation/inactivation variables, as well as time constants as a function of test potential V, as provided in [13]:

Note 2. The error due to the subjective visual inspection should not be large. I did not estimated the error, but with moving the manually placed dot over the image on the did not have consid-

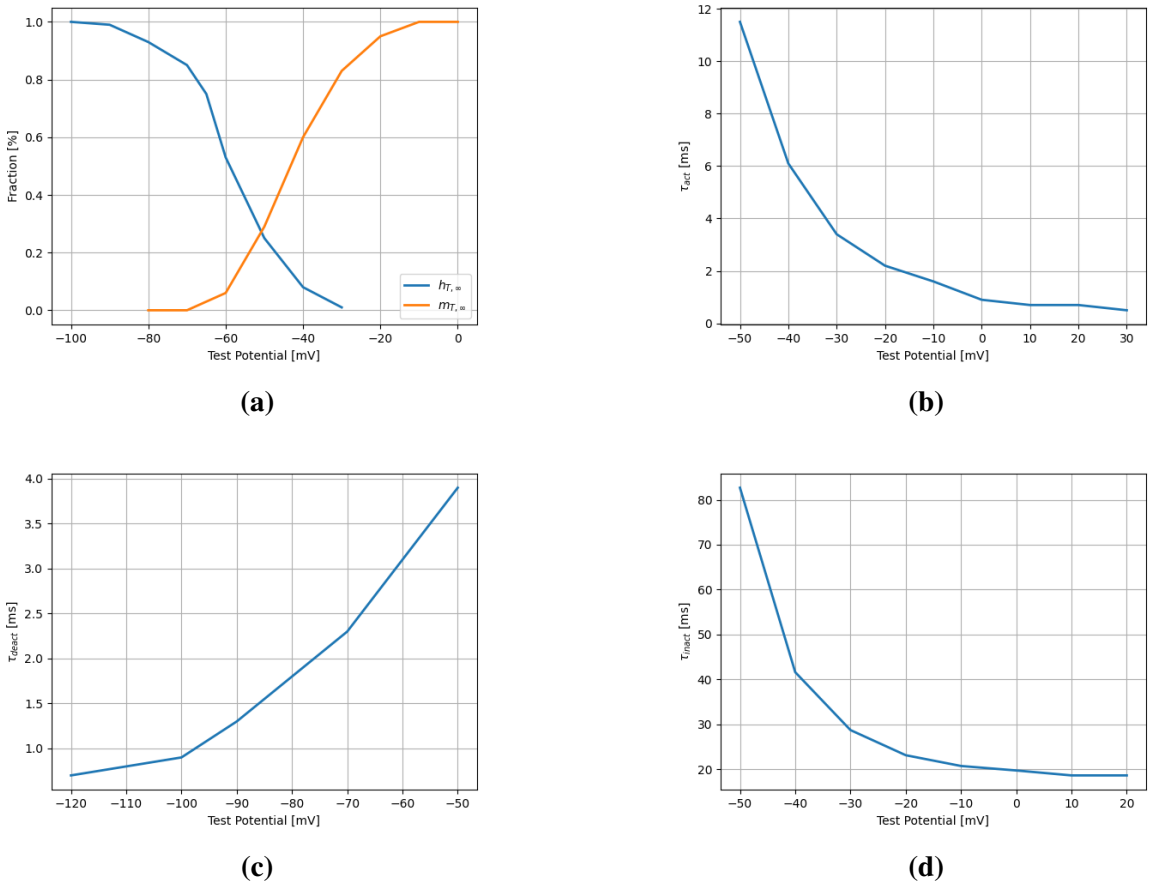

Figure 5: (a) Steady-state activation and inactivation functions of T-type Ca^{2+} channel; (b) Activation, (b) deactivation and (c) inactivation as a functions of test potentials. Data adapted from [13].

erable effect in the final values (within the moving range where the manually placed dots were not obviously not overlapping with the ones from the image).

The values of the resulted estimates (plotted in the figures above) are provided in Section **??**.

2.2.1 Estimating Steady-State Activation/Inactivation Function

Parameters for steady-state activation variable were estimated by fitting $m^3_{T,\infty}(V)$ (see Equation 2.3) to the data from electrophysiological recordings presented in [13] (similar to the procedure described in [3]). The steady-state inactivation was estimated by fitting Equation 2.8 to the data from the same paper.

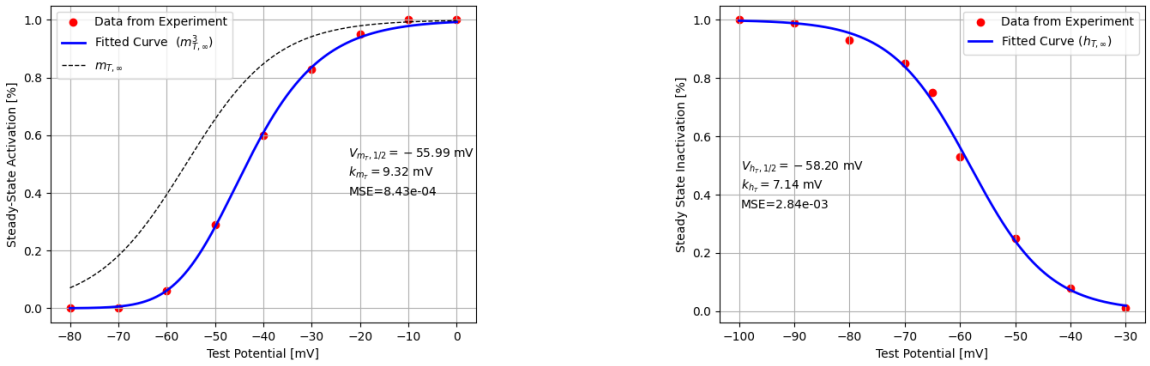

Figure 6: Fitted data to [13].

2.2.2 Estimating Activation/Inactivation Time Constants

The data was taken from [13]. The paper provides information about the values for activation/inactivation variables, as well as time constants as a functions of membrane potentials.

Activation time constant

$a_{T,1}$, $b_{T,1}$, $k_{T,1}$, $a_{T,2}$, $b_{T,2}$, $k_{T,2}$ parameters were fit to the activation ($V \geq -50$ mV) and deactivation ($V < -50$ mV) time constants provided in [13] (equations 2.5). The initial guess for the parameters were chosen to be 0, -120, 1 for $a_{T,1}$, $b_{T,1}$, $k_{T,1}$, and 0, 50, 1 for $a_{T,2}$, $b_{T,2}$, $k_{T,2}$, correspondingly. The results are shown in Figure 7a.

[13] estimated the activation time constant ($V > -50$ mV) by fitting sum of two exponentials to the recorded current trace. As it is shown in Section **??**, the fitted time constant does not

need adjustment to account for the correspondingly time constant of activation. However, the deactivation time constant needs an adjustment.

The authors estimated deactivation time constant by measuring decay of the tail current (τ_{tail}). As the model consists of three activation gates, and closing of each ion channel reuires only one activation gate to close, the deactivation time constant for one gate (out of the three) will be three times as large as τ_{tail} [9]. For this reason, τ_{m_t} for $V < -50$ mV was determined as $3 \times \tau_{\text{tail}}$.

As the set of equations 2.5 have jump discontinuity at $V = -50$mV, σ_{m_T} was introduced to model a smooth transition between the functions describing the time constant below and above -50mV (equation 2.7). The parameters of the exponentials modeling activation and deactivation time constants were fixed, and the parameter $c_{\tau_m,T}$ of σ_{m_T} was fitted to the combined data of activation and deactivation time constants from [13] (Figure 7b).

Note 3. Original paper for the base model of the R5 neuron [16] did not model the activation time constant of T-Type Ca^{2+} channels, as they replaced the activation variable by its steady state equation $m_{t,\infty}(V)$.

Note 4. [4] fitted activation time constant to double exponentials:

$$\tau_{m_T} = a_{\tau_{m_T}} + \frac{b_{\tau_{m_T}}}{\exp\left[(V - V_{\tau^1_{m_T},1/2})/k_{\tau_{m^1_T}}\right] + \exp\left[-(V - V_{\tau^2_{m_T},1/2})/k_{\tau_{m^2_T}}\right]} \tag{2.10}$$

However, MSE in case of double exponential fit was larger than with fitting the activation time constant with two exponential (see Fig.), as described above.

Inactivation time constant

[13] did not provide experimental values for τ_{h_T} below -50mV. Several authors reported recovery time constant for deinactivation to be much slower than the one of inactivation [4, 9, 10]. Equation 2.9 is a negative sigmoid, with a left asymtote at $V \approx 216$mV (Figure 8).

Note 5. Another approach would be to fit the time constant only above -50mV and take values below -50mV from another source (e.g. [9]). However, as 1) the values for Drosophila T-Type channel are not available below -50mV, 2) the fitted time constant has the same order of magnitude below -50mV as described in the literature for deinactivation time constant, 3)

given the previous comment, the exact velues will only affect time course of the current and is not very relevant for the neuronal model - continuous function was preferred for modeling the inactivation time constant.

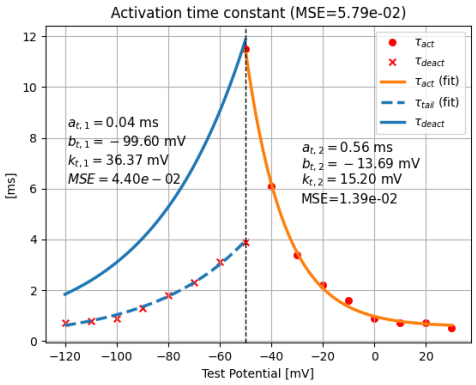

(a) Fitted activation and deactivation time constants using exponential functions

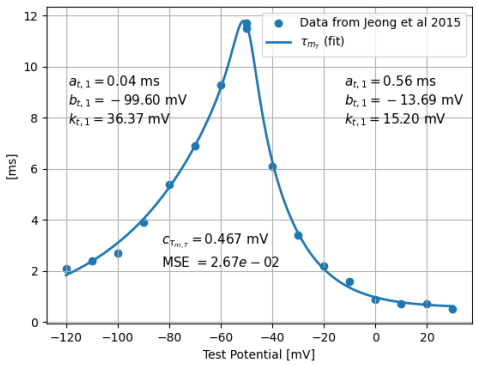

(b) Smooth transition between activation and deactivation time constants

Figure 7: Fitted τ_{m_T} to data from [13].

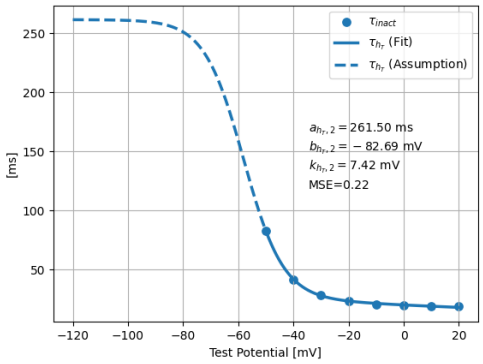

Figure 8: Fitted inactivation time constant

2.3 Simulations of T-Type Ca^{2+} Current

Simulations were done using python package '*scipy.integrate.solve_ivp*' with zero initial conditions. Different integration methods were compared: RK45, BDF, and LSODA. Each solver is optimized for different problems (stiff, non-stiff, etc.). Simulations showed, that for some cases (e.g. simulating only t-type channel) it is best to use RK45. For the simulatins presented in this section, RK45 method was used.

2.3.1 Ohmic Current vs Constant-Field Equation

- How can one fit voltage-current (I-V) relationship?
  - Ohmic current: $I(V) = g(V)(V - V_{ion})$, where $g(V) = \hat{g} m_T(V)^3 h_T(V)$, g is conductance, $\hat{g}$ maximal conductance, $m_T(V)$ ($h_T(V)$) is variable corresponding to activation (inactivation) gate.
  - Constant field equation (also known as Goldman-Hodgkin-Katz (GHK) voltage flux equation): Equation 2.1
  - The recorded voltage traces and transient I-V relationship to voltage steps is given in Figure 9.
  - Voltage step protocol: The membrane potential was held at holding potential -90 mV, followed by 150ms step pulses that varied from -80-40mV with 10mV increments (see e.g. Figure 10a, second plot from top). The response of the neuron to the voltage steps was recorded (see e.g. Figure 10a, second figure from top).
  - Observed I-V relationship was replicated for GHK model, but not for Ohmic current (Figure 10).

Add text, add captions in figure 10.

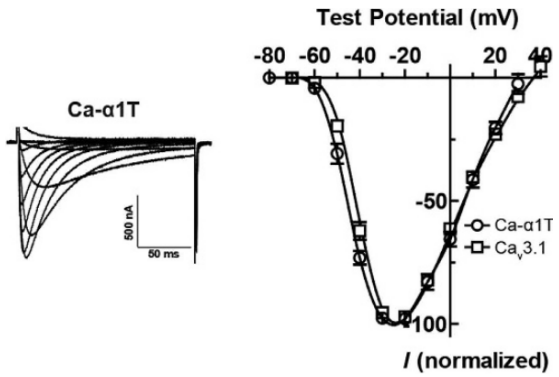

Figure 9: I-V relationship of T-Type Ca^{2+} current in Drosophila. Adapted from [13].

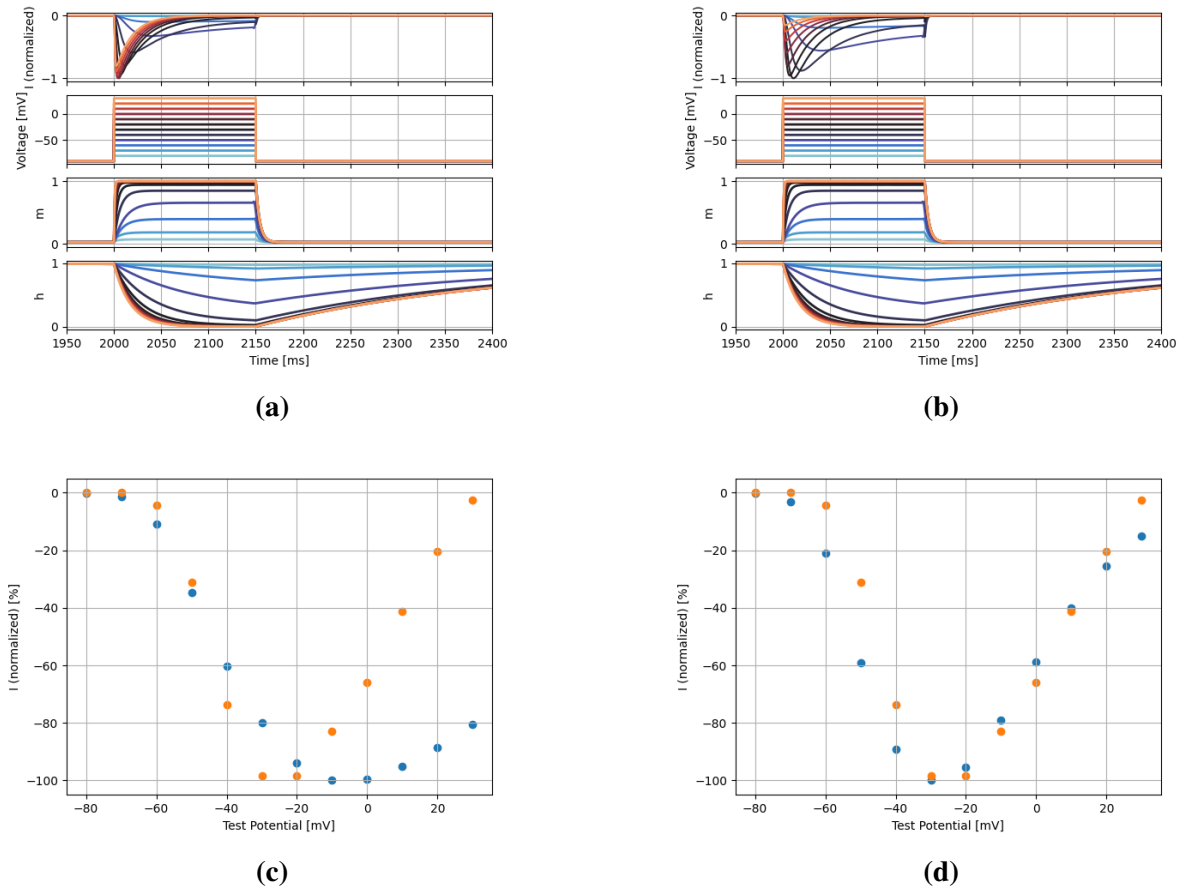

Figure 10: Ohm's low vs constant-field equation for T-Type Ca^{2+} current.

2.3.2 Scaling/Shifting Gating Variables

- $[Ca]_{outside}$, as well as solutions used during voltage-clamp experiments (calcium vs barium, as well as corresponding concentations) affects gating constants, including for mammalian homologes of Drosophila T-Type Ca channels.
- To my knowledge, how exactly the time constants are affected for Drosophila T-Type Ca channels has not been reported.
- For now: shifted steady state activation and scaled tau activation (python function curve_fit with initial guesses p0=[4, 0.5] for shift and scale correspondingly)
- m(v) to m(v-4.95)
- tau to tau*0.45

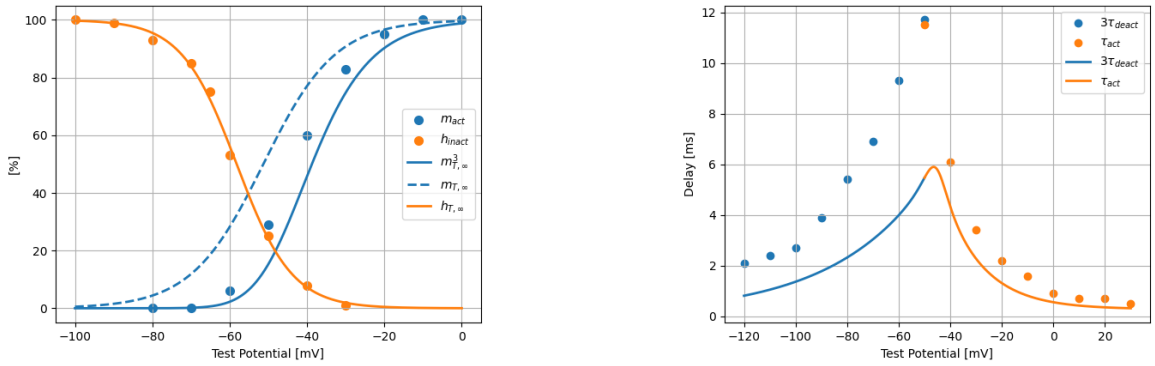

(a) **(b)**

Figure 11: Shifting and scaling time constants of activation gate

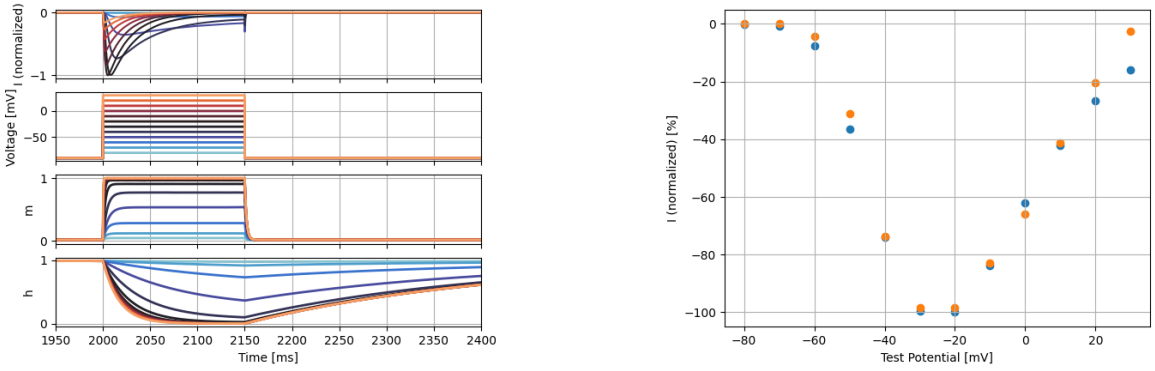

(a) **(b)**

Figure 12: Reconstructed I-V relationship after scaling and shifting activation gate time constant